Hierarchically Porous Metal Oxide Monoliths Prepared by the Nanocasting Route

Jan-Henrik Smått,[†] Claudia Weidenthaler,[‡] Jarl B. Rosenholm,[†] and Mika Lindén*,[†]

Department of Physical Chemistry, Åbo Akademi University, Porthansgatan 3-5, FIN-20500 Turku, Finland, and Department of Heterogeneous Catalysis, Max-Planck-Institut für Kohlenforschung, Kaiser-Wilhelm-Platz 1, D-45470 Mülheim an der Ruhr, Germany

Received August 22, 2005. Revised Manuscript Received January 9, 2006

In this paper, successful preparations of hierarchically porous cobalt oxide (Co_3O_4), tin oxide (SnO_2), and manganese oxide (MnO_2 or Mn_2O_3) monoliths by the nanocasting route are described. The starting SiO_2 monoliths used as molds were prepared through a straightforward sol−gel process and contain macropores with adjustable size in the range of 0.5−30 μm as well as mesopores which can be altered between 3 and 30 nm. In the nanocasting process, the silica monoliths are impregnated with a metal salt solution, which is subsequently decomposed to a metal oxide by heat treatments to form a SiO_2/MeO_x composite. Finally, the silica part can be removed by leaching in either NaOH or hydrofluoric acid. The composite and replica structures have been characterized by thermogravimetric analysis, X-ray diffraction, scanning electron microscopy, nitrogen physisorption, and transmission electron microscopy. The nanocast monoliths are positive replicas of the silica structure on the micrometer scale, meaning that the replicas have the same macroscopic morphology and macropore structure as the starting silica monoliths. In contrast, on the nanometer scale the replicated structure becomes an inverse (or a negative replica) of the silica mesopore structure. Furthermore, all prepared metal oxide monoliths are fully crystalline. When the hierarchical structure of the monoliths is combined with the unique chemical or physical properties of the used metal oxides, these novel materials have great potential in application areas such as catalysis, HPLC, and sensor materials.

1. Introduction

High surface area metal oxides are of great importance in many applications, including catalysis, electronics, and sensor technology.[1−6] These materials could, for instance, have interesting electric, magnetic, or thermal properties or could be chemically resistant in harsh environments. Most of the mesoporous non-siliceous oxide materials produced to date are available in the form of powders or films. However, monolithic silica, especially monoliths exhibiting a multimodal porosity, has gained a lot of recent interest.[7−11] The advantage of these types of hierarchical materials is that the large macropores combined with the mesopore structure give the monoliths large transport channels accompanied by a high active surface area.

A great number of hierarchically structured silica materials have already been described, including monoliths and spray dried powders.[7−11] Recently, Nakanishi and co-workers have developed a sol−gel method to prepare macroporous/mesoporous silica monoliths.[8] The idea is to induce phase separation that takes place at the sol−gel transition, which can be done by adding a hydrogen bonding polymer (such as poly(ethylene oxide)) to the sol. After removing the liquid phase a macroporous body is obtained. Additionally, textural mesopores from voids between particles are also present. The size of these pores can be controlled separately by post-solvent exchange treatments in ammonia.[12] Furthermore, surfactants such as cetylammonium salts or block copolymers can also be added to induce a trimodal pore structure.[9,10] These kinds of structures are well-suited as support materials in catalysis or HPLC,[13] where a low pressure drop over the material is needed.

However, in many applications hierarchical materials with chemical and physical properties other than the ones observed for silica are required. For example, amorphous silica cannot be used in harsh conditions such as extreme pH values or high temperatures because of its high solubility.[14] However, it is not a trivial task to generalize the "phase separation

* To whom correspondence should be addressed. Fax: +358-2-215 4706. Tel.: +358-2-215 2355. E-mail: mlinden@abo.fi.
† Åbo Akademi University.
‡ Max-Planck-Institut für Kohlenforschung.

(1) Tosheva, L.; Valtchev, V. P. *Chem. Mater.* **2005**, *17*, 2494.
(2) Stein, A. *Adv. Mater.* **2003**, *15*, 763.
(3) Taguchi, A.; Schüth, F. *Microporous Mesoporous Mater.* **2005**, *77*, 1.
(4) Schüth, F. *Chem. Mater.* **2001**, *13*, 3184.
(5) Scott, B. J.; Wirnsberger, G.; Stucky, G. D. *Chem. Mater.* **2001**, *13*, 3140.
(6) Sanchez, C.; Lebeau, B.; Chaput, F.; Boilot, J. P. *Adv. Mater.* **2003**, *15*, 1969.
(7) Sen, T.; Tiddy, G. J. T.; Casci, J. L.; Anderson, M. W. *Chem. Mater.* **2004**, *16*, 2044.
(8) Nakanishi, K. *J. Porous Mater.* **1997**, *4*, 67, and references therein.
(9) Smått, J.-H.; Schunk, S.; Lindén, M. *Chem. Mater.* **2003**, *15*, 2354.
(10) Shi, Z. G.; Feng, Y. Q.; Xu, L.; Da, S. L.; Ren, Y. Y. *Microporous Mesoporous Mater.* **2004**, *68*, 55.
(11) Lind, A.; du Fresne von Hohenesche, C.; Smått, J.-H.; Lindén, M.; Unger, K. K. *Microporous Mesoporous Mater.* **2003**, *66*, 219.
(12) Nakanishi, K.; Nagakane, T.; Soga, N. *J. Porous Mater.* **1998**, *5*, 103.
(13) Ishizuka, N.; Minakuchi, H.; Nakanishi, K.; Soga, N.; Tanaka, N. *J. Chromatogr., A* **1998**, *797*, 133.

10.1021/cm051880p CCC: $33.50
Published on Web 02/16/2006

method" to other metal oxides with a few exceptions (SiO_2/TiO_2 and SiO_2/ZrO_2 mixtures[8] or TiO_2[15]), because many metal oxide precursors are not available as alkoxides and the rates of hydrolysis and condensation are often very high.

Several ways to avoid these problems have been described in the literature. Stein et al. and later a number of other groups have been using closely packed latex spheres as hard templates for producing three-dimensionally ordered macroporous materials,[16] while the group of Seshadri has produced macroporous materials from crystalline single-source precursors through decomposition followed by selective leaching of one of the phases.[17] The major drawbacks of these materials are the small window sizes between the cagelike macropores combined with high production costs due to expensive templates in the first system and the limited mesoporosity in the latter. Furthermore, by using anion-exchange resins as macrotemplates a wide variety of inorganic spheres have been prepared, including different zeolite structures.[18,19] Here, the morphology is restricted to macroscopic beads.

Silica has proven to be an excellent starting (scaffold) material in nanocasting procedures. For instance, it has been shown that mesoporous silica powders can be used as molds *or hard templates* for making mesoporous carbon [20,21] or non-siliceous oxide[22−25] replicas. In nanocasting of carbon, the starting silica materials are impregnated with an organic monomer, which is polymerized and subsequently carbonized, and the result is a silica/carbon composite. A negative carbon replica can be obtained by leaching out the silica phase with hydrofluoric acid (HF). The method has also successfully been expanded to replicate macroporous/mesoporous silica monoliths.[26−29] A similar technique has been used in the preparation of metal oxide replicas of mesoporous silica powders.[22−25] Here, the silica material is impregnated with a metal salt solution. The metal salt is decomposed to an oxide by heat treatments, upon which the silica part can be leached out with either NaOH or HF. Many different metal oxides (Cr_2O_3,[22,25] In_2O_3,[23,25] CeO_2,[24,25] NiO,[25] MnO_x,[25] Co_3O_4,[25] Fe_2O_3[25]) have successfully been prepared by nanocasting of mesoporous silica, resulting in a negative replica on the nanometer scale. The limitation of this method is that the desired metal oxide has to be resistant toward leaching in NaOH and/or HF to make it possible to remove the silica part selectively.

Recently, we succeeded in replicating the macroporous/mesoporous silica monoliths described above into cobalt oxide monoliths with a similar macroporous structure.[30] In this paper we will report more extensive work on the cobalt oxide replicas and demonstrate that it is possible to expand the method to other metal oxides as well, such as manganese oxide and tin oxide. The final structure is much dependent on the metal salt used and the processing parameters. Furthermore, we have also studied which effect the structure of the parent silica monoliths has on the replica structure. The unique combination of the chemical, physical, and morphological properties of the metal oxide monoliths makes them suitable for a large number of application areas such as separation, catalysis, semiconductors, and many others.

2. Experimental Section

2.1. Materials. For the preparation of macroporous silica monoliths poly(ethylene glycol) (PEG, $M_w = 35\,000$ g mol^{-1}, Merck), nitric acid (30%), tetraethyl orthosilicate (TEOS, 98%, Aldrich) and cetyltrimethylammonium bromide (CTAB, Aldrich) were used. In the nanocasting procedure $Co(NO_3)_2 \cdot 6H_2O$ (98%, Fluka), $SnCl_2 \cdot 2H_2O$ (98%, Fluka), and $Mn(NO_3)_2 \cdot 4H_2O$ (97%, Fluka) were used as metal oxide precursors.

2.2. Synthesis. Bimodal macroporous/mesoporous silica monoliths were prepared according to previously described procedures.[8,9] First, PEG was dissolved in H_2O and HNO_3 (30%). TEOS was then added, and the solution was stirred until a clear and homogeneous solution was obtained. The H_2O/HNO_3/TEOS/PEG(35 000) molar ratio in the final sol was $14.7{:}0.25{:}1{:}7.8 \times 10^{-4}$. To investigate the replication mechanism in more detail an additional type of monolithic silica structure was used as the mold in the nanocasting of SnO_2 monoliths. These silica monoliths have an additional pore size region of about 3 nm induced by supramolecular templating of CTAB.[9] The starting H_2O/HNO_3/TEOS/PEG(35 000)/CTAB molar ratio of these monoliths was $14.7{:}0.25{:}1{:}4.3 \times 10^{-4}{:}0.14$. (Samples prepared from this type are denoted CTAB−). The solutions were portioned into micro-titer plates and were allowed to gel and age for 72 h at 40 °C. Solvent exchange in a 1 M NH_4OH solution for 24 h at 90 °C was performed to increase the stability of the monoliths and to adjust the textural mesopore size. The monoliths were subsequently dried at 40 °C for 72 h and finally calcined at 550 °C for 5 h with a heating ramp of 1 K/min. The resulting SiO_2 monoliths have an approximate size of ∅ 5 × 7 mm after the calcination step.

The nanocasting procedures are schematically described in Figure 1. Aqueous solutions of metal salts were prepared according to Table 1. Outgassed silica monoliths were impregnated by incipient wetness. The wet, fully transparent monoliths were placed on crucibles and heated directly at 150 °C for 10 h ($Co(NO_3)_2 \cdot 6H_2O$ and $Mn(NO_3)_2 \cdot 4H_2O$) or 150 °C for 4 h and then 250 °C for 4 h ($SnCl_2 \cdot 2H_2O$). The impregnation and heating steps were repeated two to four times depending on which salt was used. Subsequently, the composites were calcined in air at 550 °C (or 300 °C for MnO_2) for 6 h with a heating ramp of 1 K/min. Finally,

(14) Iler, R. K. *The Chemistry of Silica*; Wiley-Interscience: New York, 1979.
(15) Fujita, K.; Konishi, J.; Nakanishi, K.; Hirao, K. *Appl. Phys. Lett.* **2004**, *85*, 5595.
(16) Blanford, C. F.; Yan, H.; Schroden, R. C.; Al-Daous, M.; Stein, A. *Adv. Mater.* **2001**, *13*, 401.
(17) Rajamathi, M.; Thimmaiah, S.; Morgan, P. E. D.; Seshadri, R. *J. Mater. Chem.* **2001**, *11*, 2489.
(18) Tosheva, L.; Valtchev, V.; Sterte, J. *Microporous Mesoporous Mater.* **2000**, *35−36*, 621.
(19) Naydenov, V.; Tosheva, L.; Sterte, J. *Microporous Mesoporous Mater.* **2003**, *66*, 321.
(20) Ryoo, R.; Joo, S. H.; Jun, S. *J. Phys. Chem. B* **1999**, *103*, 7743.
(21) Jun, S.; Joo, S. H.; Ryoo, R.; Kruk, M.; Jaroniec, M.; Liu, Z.; Ohsuna, T.; Terasaki, O. *J. Am. Chem. Soc.* **2000**, *122*, 10712.
(22) Zhu, K.; Yue, B.; Zhou, W.; He, H. *Chem. Commun.* **2003**, *1*, 98.
(23) Yang, H.; Shi, Q.; Tian, B.; Lu, Q.; Gao, F.; Xie, S.; Fan, J.; Yu, Ch.; Tu, B.; Zhao, D. *J. Am. Chem. Soc.* **2003**, *125*, 4724.
(24) Laha, S. C.; Ryoo, R. *Chem. Commun.* **2003**, *17*, 2138.
(25) Tian, B.; Liu, X.; Yang, H.; Xie, S.; Yu, Ch.; Tu, B.; Zhao, D. *Adv. Mater.* **2003**, *15*, 1370.
(26) Taguchi, A.; Smått, J.-H.; Lindén, M. *Adv. Mater.* **2003**, *15*, 1209.
(27) Shi, Z. G.; Feng, Y. Q.; Xu, L.; Da, S. L.; Zhang, M. *Carbon* **2003**, *41*, 2677.
(28) Lu, A.-H.; Smått, J.-H.; Backlund, S.; Lindén, M. *Microporous Mesoporous Mater.* **2004**, *72*, 59.
(29) Lu, A.-H.; Smått, J.-H.; Lindén, M. *Adv. Funct. Mater.* **2005**, *15*, 865.
(30) Smått, J.-H.; Spliethoff, B.; Rosenholm, J. B.; Lindén, M. *Chem. Commun.* **2004**, *19*, 2188.

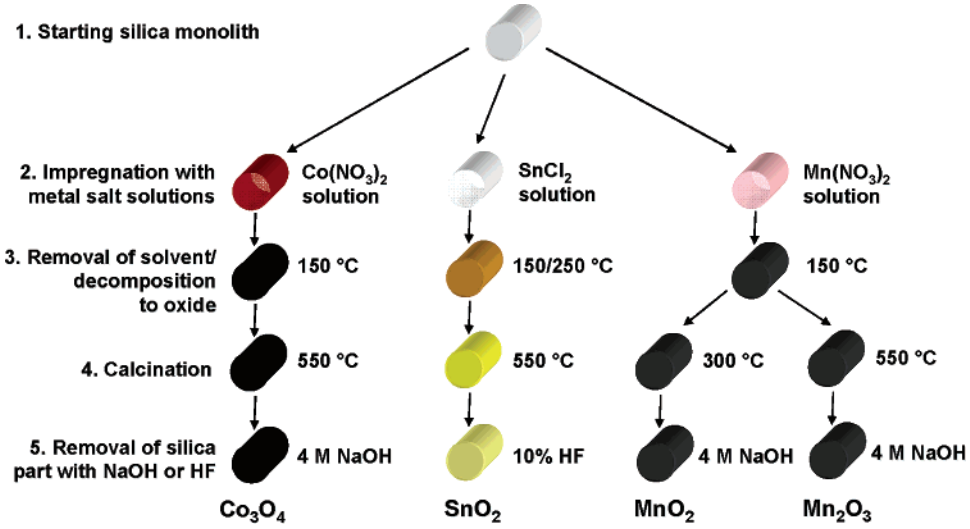

Figure 1. Synthesis scheme of the preparation of different metal oxides. The starting silica monoliths have both macro- and mesopores, which initially will be filled with the metal salt solution.

Table 1. Starting Metal Salt Concentrations in the Nanocasting Procedure Together with the Number of Impregnation Steps and the Total Mass Increase in the Composite[a]

metal oxide	precursor	concentration [wt %]	concentration [M]	no. impregnations	% mass[b] increase	BET surface area [m^2/g]	mesopore volume [cm^3/g]	mesopore diameter[c] [nm]
SiO_2						243.9	1.268	23.6
CTAB−SiO_2						938.0	1.293	2.9/22.3
SiO_2/Co_3O_4	$Co(NO_3)_2 \cdot 6H_2O$	78.6	5.34	3	293.5	44.8	0.137	15.1
SiO_2/SnO_2	$SnCl_2 \cdot 2H_2O$	66.7	6.72	3	516.0	12.2	0.044	20.9
SiO_2/MnO_2	$Mn(NO_3)_2 \cdot 4H_2O$	50.0	3.10	5	323.7	55.2	0.142	13.5
SiO_2/Mn_2O_3	$Mn(NO_3)_2 \cdot 4H_2O$	50.0	3.10	5	296.3	55.8	0.173	14.8
CTAB−SiO_2/SnO_2	$SnCl_2 \cdot 2H_2O$	66.7	6.72	3	625.1	10.6	0.012	2.7/14.0

[a] Nitrogen physisorption data of the starting silica as well as the composites are reported. [b] The % mass increase of the composites was calculated using the formula: $[(m_{composite} - m_{silica})/m_{silica}] \times 100$. [c] Estimated from the BJH desorption plot.

the silica part was removed by dissolution in either 4 M NaOH (at 90 °C, 2 × 24 h) or 10% HF (at room temperature, 24 h).

2.3. Characterization. Thermogravimetric analysis (TGA) and differential temperature analysis (DTA) on a Netzsch STA 449 C thermobalance were applied to determine the combustion temperatures of the different metal salts. The measurements were done on dried metal salt/silica composites in air with a heating ramp of 10 K/min. Furthermore, X-ray diffraction (XRD) patterns were measured to determine the crystalline phases of the metal oxide replicas. The samples were measured on a PANalytical X'Pert Pro Bragg−Brentano system (used wavelength Cu $K\alpha_{1,2}$), equipped with a secondary monochromator and a X'Celerator detector (PDS length 2.12° 2θ). The data were collected in the range between 10 and 90° 2θ with a step width of 0.02° 2θ. The data collection of the MnO_2 sample was performed with a Stoe Bragg−Brentano diffractometer (used wavelength Cu $K\alpha_{1,2}$). The samples were ground in a mortar prior to the preparation in the sample holder. The particle size was also estimated from the XRD measurements by using the Scherrer equation.[31] Fracture surfaces of the monoliths were examined by a scanning electron microscope (LEO type Stereoscan 360, U.K.) equipped with a Link Inca 300 (Oxford Instruments, U.K.) EDS unit, which was used for the elemental analysis. The samples were coated by platinum prior to analysis. The mesopores were studied with a transmission electron microscope (Hitachi HF2000, equipped with a cold field emission gun) as well as nitrogen physisorption (ASAP 2010, Micromeritics). The BET surface area was determined from the relative pressure range $P/P_0 = 0.05-0.20$, and the total mesopore volume was determined from the adsorption branch at $P/P_0 \sim 0.98$. The pore volume is only to be taken as an approximation, because the pore sizes are too large to be properly measured by nitrogen sorption. The pore size distribution was calculated using the BJH method based on the desorption branch.

(31) Langford, J. I.; Wilson, A. J. C. *J. Appl. Crystallogr.* **1978**, *11*, 102.

3. Results and Discussion

3.1. Nanocasting Procedure. The synthesis and the structure of the parent SiO_2 monoliths have been described elsewhere.[8,9]

As described in Experimental Section and in Figure 1, the nanocasting procedure is a straightforward method to prepare macroporous metal oxide monoliths. Typically metal nitrates were used as metal oxide precursors because of their high solubility in water and their low decomposition temperatures. In the case of tin oxide, $SnCl_2 \cdot 2H_2O$ was used because no commercial tin nitrate was available. The concentrations of the metal salt precursor solutions were typically saturated or close to saturated. The concentration of the precursor solution plays an important role for the evolution of the structure, as will be discussed later. More importantly, it was found out that the "removal of solvent/decomposition to oxide" step (number 3 in Figure 1) was the most crucial step for determining the final structure and for the mechanical stability of the replicas. A direct heat treatment at 150 °C was used for all three metal oxide precursors to remove the solvent from the interior of the monoliths. If too high or too low temperatures are used, different sorts of problems may arise. If the monoliths are dried at temperatures too low, large crystals of the metal salt will form inside the pores, which

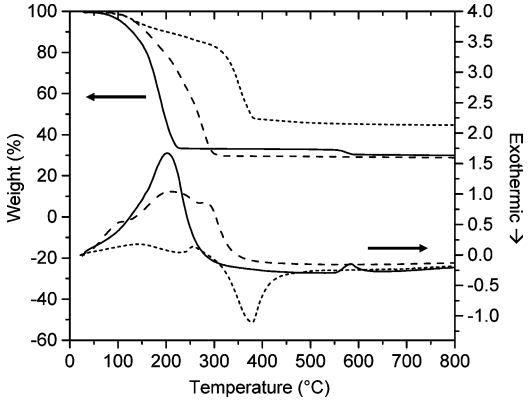

Figure 2. TGA and DTA of dried impregnated monoliths: $Co(NO_3)_2 \cdot 6H_2O$ (dashed lines), $SnCl_2 \cdot 2H_2O$ (dotted lines), and $Mn(NO_3)_2 \cdot 4H_2O$ (solid lines). As a result of the different metal oxide loading amounts the weight contribution from the silica part has been removed, using the % mass increase values given in Table 1.

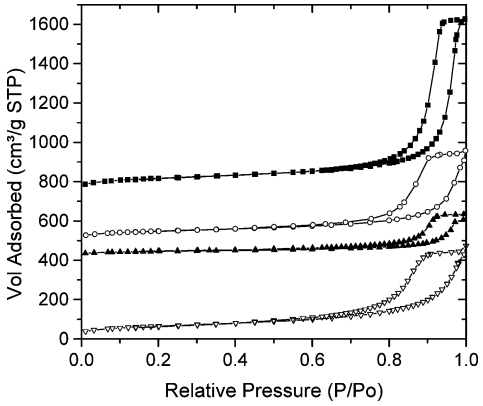

Figure 3. Nitrogen physisorption isotherms of the parent SiO_2 monolith (■; offset, 750 cm^3/g), as well as the SiO_2/Co_3O_4 composite (○; offset, 500 cm^3/g), the SiO_2/SnO_2 composite (▲; offset, 425 cm^3/g), and finally the SiO_2/MnO_2 composite (▽). Note: the composite isotherms have been corrected for the weight increase upon impregnation, using the % mass increase values given in Table 1.

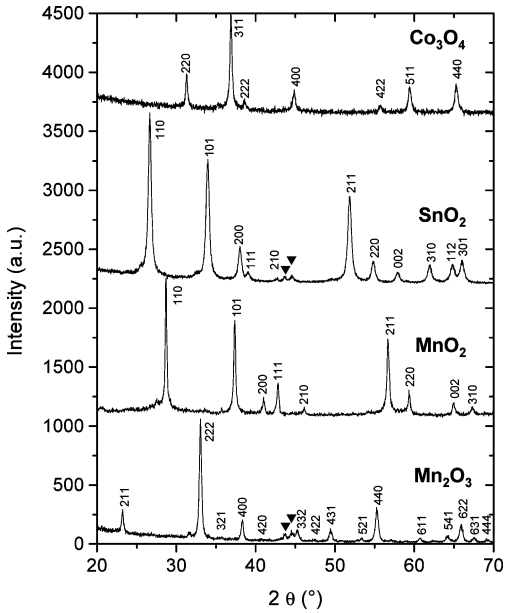

Figure 4. XRD indicates that the final metal oxide phases are Co_3O_4, SnO_2, MnO_2, and Mn_2O_3. ▼ indicates reflections associated with the sample holder.

will eventually lead to macroscopic cracks in the monolithic body. On the other hand, if the drying temperature is too high, problems with diffusion of salt molecules from the center of the monoliths are often encountered, which result in hollow replicas. Depending on the type of metal salt used in the process, the temperature may need to be adjusted to successfully decompose the salts to oxides. As seen in the TGA/DTA plot in Figure 2, the nitrate salts of cobalt and manganese decompose at relatively low temperatures (complete decomposition between 200 and 300 °C), while a pronounced mass loss is not observed before 370 °C for the $SnCl_2$ sample. It should be noted that if longer treatments are used, lower temperatures are needed for the nucleation and growth of the oxide phase. Furthermore, it was found out that the salts do not have to be fully decomposed between the impregnation steps. This explains the choice of 150 °C to decompose the nitrates while the slightly higher temperature of 250 °C was used to decompose the tin chloride. The *drying* and the *decomposition* steps are closely interlinked, and they take place simultaneously. This implies it is not a trivial task to generalize this step for the preparation of monoliths of other metal oxides. The results will also strongly depend on the atmosphere inside the oven. By repeating the impregnation steps two to four times, the integrity of the replica structures could be enhanced. As a rule of thumb, more than 50% of the mesopores should be filled to provide a rigid structure.

After the final impregnation step the composites were calcined at 550 °C (except MnO_2 which was calcined at 300 °C) to make the decomposition go to completion. Interestingly, a small mass loss of about 10 wt % can be observed in the TGA plot at ∼580 °C, which we ascribe the mass loss associated with the phase transition from MnO_2 to Mn_2O_3. After the calcination step the degree of loading of the mesopores in the composites was studied with nitrogen sorption measurements. The parent silica monoliths have textural mesopores which originate from voids between the primary silica particles. Like it has been described in previous reports, it is possible to tune the size of these pores by post-treatments in ammonia solutions of different concentrations or temperatures.[12] In our case, the post-treatment was chosen to create mesopores of about 20 nm. In Figure 3, the nitrogen sorption isotherms of the composites have been plotted together with the parent silica isotherm. Note that the isotherms for the composites have been normalized for clarity, taking into account the total weight increase. The values for the respective mass increases given in Table 1 were used as the basis for normalization. What is common for all three composites is that the nitrogen uptake in the relative pressure range between 0.8 and 1.0 decreases, which indicates that the textural mesopores in the silica monoliths are gradually being filled, isotherms are normalized against the increase in specific weight upon impregnation. From the isotherms, the specific surface area, pore volume, and pore size distribution could be determined as well (Table 1). Both the SiO_2/Co_3O_4 and the SiO_2/MnO_2 composites show a broadened hysteresis loop indicating that the mesopores are partially blocked.

After the SiO_2 part had been removed, the phase composition of the samples was determined by XRD measurements. The diffractograms are presented in Figure 4. It was

Table 2. Nitrogen Physisorption Data of the Starting Silica Monoliths Together with the Metal Oxide Replicas and Estimations of the Particle Sizes of the Different Metal Oxides

sample	BET surface area [m^2/g]	mesopore volume [cm^3/g]	mesopore diameter[a] [nm]	particle size diameter TEM [nm]	particle size diameter N_2[b] [nm]	particle size diameter XRD [nm]
SiO_2	243.9	1.268	23.6	5−20	11.2	
CTAB−SiO_2	938.0	1.293	2.9/22.3		2.9	
Co_3O_4	40.4	0.119	12.3[c]	10−20	24.4	20−30
SnO_2	36.0	0.111	7.8[c]	7−15	24.0	15−20
MnO_2	35.9	0.098	5−30	not measured	33.2	not measured
Mn_2O_3	29.8	0.075	10−35	15−30	44.8	30−35
CTAB−SnO_2	70.4	0.108	2−100	3−7/15−35	12.3	mean ∼ 16

[a] Estimated from the BJH desorption plot. [b] The particle size diameter determined from the BET areas was calculated using the following formula: $d = 6/(A_{BET}\delta)$. [c] The pore sizes of the silica templated mesopores.

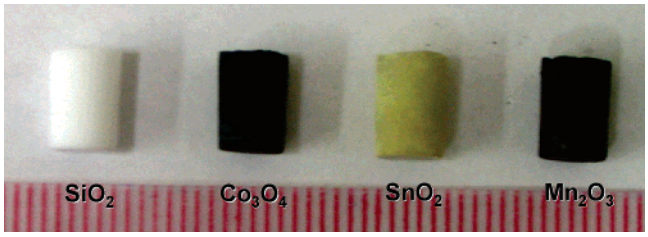

Figure 5. Photograph of the parent SiO_2 monolith together with Co_3O_4, SnO_2, and Mn_2O_3 replicas (scale bar in millimeters).

discovered that calcining monoliths impregnated with $Co(NO_3)_2 \cdot 6H_2O$ in air resulted in the formation of Co_3O_4 while SnO_2 was obtained when $SnCl_2 \cdot 2H_2O$ was calcined. Depending on the calcination temperature, relatively pure phases of both MnO_2 (300 °C) and Mn_2O_3 (550 °C) could be obtained from $Mn(NO_3)_2 \cdot 4H_2O$. There are some additional reflections in the manganese oxide patterns, which we have not been able to assign. The Scherrer equation was used to estimate the crystallite size of the replicas (see Table 2), and the results will be discussed in more detail later. Furthermore, energy-dispersive X-ray (EDX) analysis was used to quantify the residual silica in the metal oxide replicas, which was determined to be less than 1 wt %.

3.2. Structure of the Metal Oxide Replicas. By using the methods described above mechanically stable metal oxide monoliths were obtained upon the removal of the silica portion. Typical examples of a parent silica monolith and three different metal oxide replicas are represented in Figure 5. An interesting feature is that virtually no shrinkage can be observed for any of the replicas. This means that by changing the morphology of the parent silica monoliths it is possible to control the morphology of the monolithic replicas as well. The final Co_3O_4 monoliths are black, while the SnO_2 and Mn_2O_3 replicas are yellow-beige and dark gray, respectively. The colors are homogeneously distributed throughout the interior of the monoliths as well, which indicates a high degree of chemical homogeneity, as also confirmed by EDX analysis.

When looking closer at the interior of the monoliths with scanning electron microscopy (SEM), it is evident that the silica monoliths as well as the replicas are macroporous (Figure 6). As shown in previous reports, it is fairly simple to control the pore size in macroporous silica monoliths.[8,9] The macropores are formed by phase separation, induced by a hydrogen bonding polymer (PEG) at the same instant as the sol−gel transition. Thus, by changing the PEG amount the pore size can be adjusted in the range of 0.5−30 μm. In our case, the PEG concentration was chosen to give macropores of roughly 3−6 μm in diameter (estimated from the SEM image in Figure 6a). Interestingly, the nanocasted

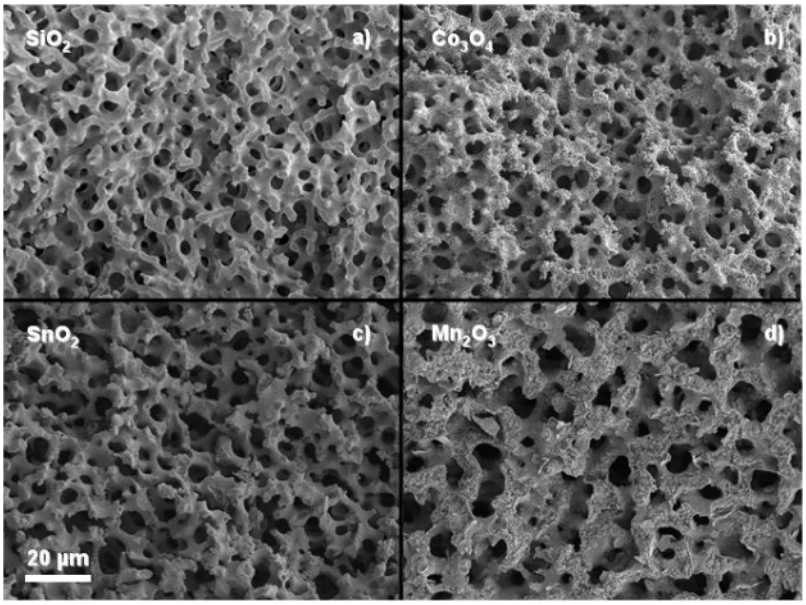

Figure 6. SEM images of (a) the parent SiO_2 monolith, (b) the Co_3O_4 replica, (c) the SnO_2 replica, and (d) the Mn_2O_3 replica (slightly larger macropores in the starting silica monolith).

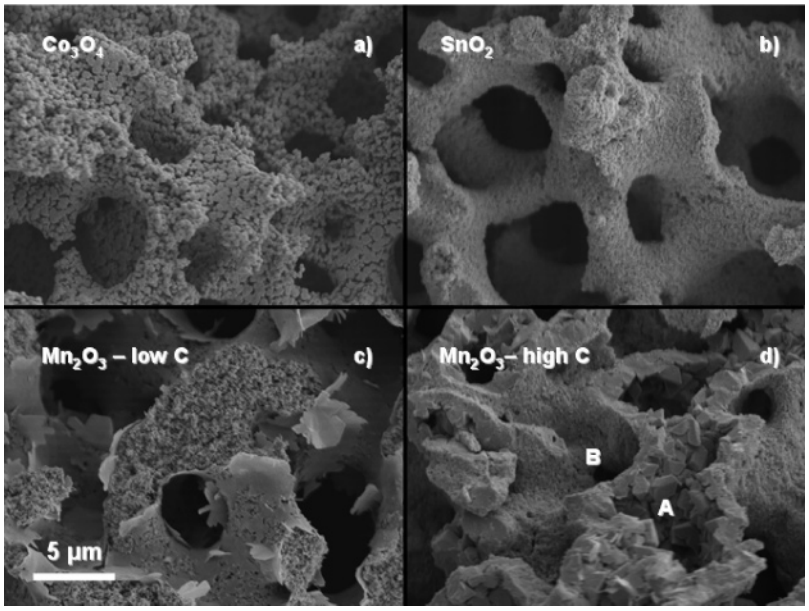

Figure 7. SEM images of the (a) Co_3O_4, (b) SnO_2, and (c) Mn_2O_3 replicas, which show the porous macropore walls. (d) A Mn_2O_3 replica with too high of a starting $Mn(NO_3)_2$ concentration. Point A indicates a former macropore half-filled with large Mn_2O_3 crystals, while point B represents the former silica wall which has been dissolved in NaOH.

monoliths have virtually the same pore size (Figure 6). Hence, it is evident that the macropores are only initially filled with salt solution, and when the solvent evaporates from the pores the metal oxide precursors will preferentially diffuse into the mesopores. This means that the metal oxide monoliths are positive replicas on the micrometer scale. It also indicates that, by changing the macropore structure of the silica monolith, the pore size of the replicas can be altered.

Even if the macropore size is practically the same for all replicas, the structures of the macropore walls somewhat differs from each other. The parent silica has got relatively smooth walls, which is also the case of the tin oxide replica. On the other hand, the cobalt and the manganese oxides have a rougher wall structure, which can be seen in the SEM images in Figure 7. The Co_3O_4 replica consists of large "spherical" aggregates of particles (∼150 nm) (Figure 7a and transmission electron microscopy (TEM) image in Figure 9a), while the Mn_2O_3 replica has slightly smaller aggregates (Figure 7c). The voids between the aggregates in the Co_3O_4 and Mn_2O_3 replicas can also be observed in the mercury porosimetry measurements (results not shown). The inter-aggregate voids in Co_3O_4 and Mn_2O_3 are ∼250 nm and ∼150 nm, respectively. The size of the inter-aggregate voids is bound to be controlled by several factors, including the respective relative nucleation and growth kinetics, the number of impregnation/decomposition cycles, and the drying/decomposition temperature. In Figure 7c,d the structures of two Mn_2O_3 replicas with low and high $Mn(NO_3)_2$ starting concentrations are shown. If the concentration is too high, large crystals are formed on the outside of the macropore walls and the manganese nitrate cannot enter the mesopores. When the silica part is leached the material has no replicated mesopores and a low surface area. On the other hand, if concentrations that are too low are used the drawbacks are the greater diffusion of the metal salt from the center of the monoliths and the larger number of impregnations needed to reach a rigid structure. The structure on this level can still be said to be a positive replica of the silica structure.

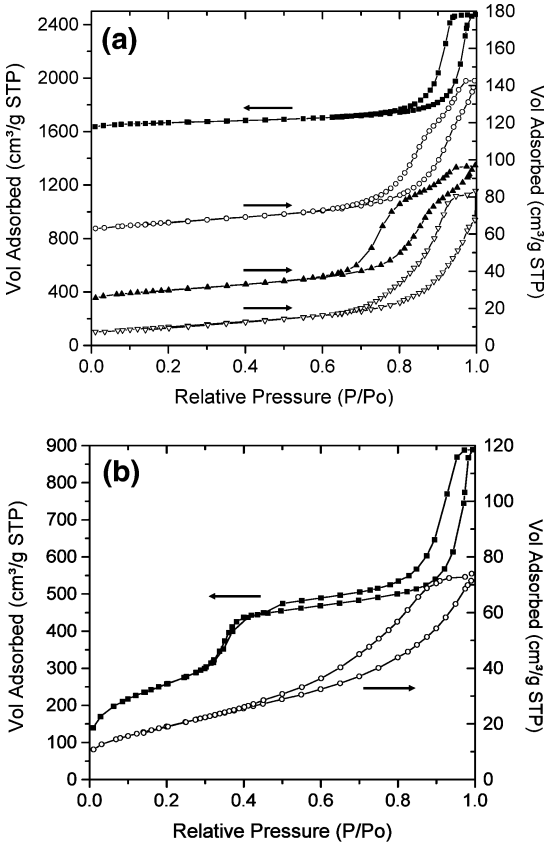

Figure 8. a) Nitrogen physisorption isotherms of the parent SiO_2 monolith (■, left scale bar; offset, 1600 cm^3/g), as well as the Co_3O_4 replica (○, right scale bar; offset, 55 cm^3/g), the SnO_2 replica (▲, right scale bar; offset, 20 cm^3/g), and the MnO_2 replica (▽, right scale bar). (b) Nitrogen physisorption isotherms of the parent CTAB−SiO_2 monolith (■, left scale bar) together with the CTAB−SnO_2 replica (○, right scale bar).

By zooming in closer on the macropore walls one can observe yet another pore size region, the textural mesopores. In Figure 8a the nitrogen sorption isotherms of the parent

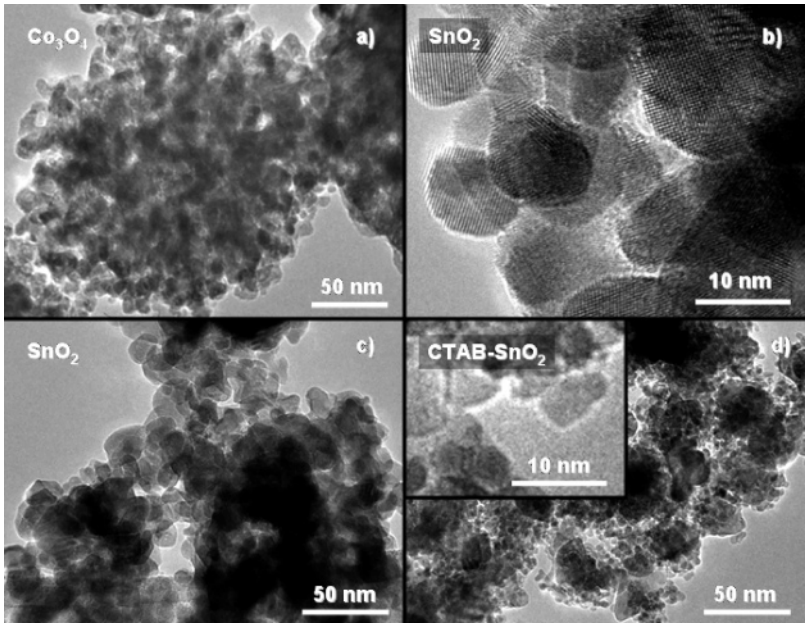

Figure 9. TEM images: (a) particle aggregates of the Co_3O_4 replica; (b) both the particle size and the atomic order of the SnO_2 replica; and (c) the SnO_2 replica of monomodal SiO_2 and (d) of bimodal SiO_2 (inset, zoomed-in view of part d).

SiO_2 together with the different replicas are plotted (note the two different scales on the ordinate). Here, one can see that the nitrogen uptake between 0.9 and 1.0, which could be observed in the respective composites, is still present for all replicas. However, for SnO_2 another uptake between 0.8 and 0.9 can clearly be observed. The same effect may also be seen for both the Co_3O_4 and the MnO_2 replicas. However, in the case of the manganese oxide only a broad uptake can be observed instead of two distinctive steps as can be seen for the other oxides. A comparable phenomenon was observed when carbon replicas were made of the same type of silica monoliths.[29] These pores are formed by the templating of the silica structure, and the formed structure is a negative replica of the silica structure.

To verify the theory a second type of silica monolith (CTAB−SiO_2) containing a trimodal pore structure was used as the mold in the nanocasting of tin oxide monoliths (CTAB−SnO_2). These silica monoliths have apart from macropores two mesopore regions (∼3 nm and ∼20 nm) instead of just one as in the ones previously discussed.[9] By comparing the nitrogen sorption isotherms of the starting silica and the SnO_2 replica we can see very large differences between the two (Figure 8b). The silica monolith has two very distinct steps at $P/P_0 = 0.3-0.4$ and $P/P_0 = 0.9-1.0$ in the isotherm indicating the bimodal mesopore structure, while the replica only has one very broad uptake covering almost the entire relative pressure range. This can be explained by the broad wall size distribution of the surfactant templated mesopores in the silica structure (no ordered mesopores), which will become the pores in the metal oxide replica. This does not mean that the replication has failed, but on the contrary, a structure with a bimodal *particle* size distribution has formed, which is confirmed by the TEM images in Figure 9c,d. Similar structures could also be observed in carbon replicas of the same type of silica monoliths.[28] The extracted specific surface areas, pore volumes, and pore size distributions are presented in Table 2. The specific surface areas and the total pore volumes of the replicas are remarkably lower than those of the parent silica monolith, but one should still keep in mind that the densities of the metal oxides are more than two to three times higher than those of amorphous silica.

The mesopore structure of the replicas was also closer studied by TEM. Figure 9a represents one of the Co_3O_4 aggregates earlier seen in the SEM image in Figure 7a. Each of these grains consists of loosely packed particles in the size range of 10−20 nm. From the TEM image in Figure 9b one can see that the SnO_2 replica consists of much smaller particles (7−15 nm). The Mn_2O_3 monoliths (not shown) have the largest particles (15−30 nm). As already mentioned, SnO_2 replicas prepared from silica monoliths with different mesopore structures were studied as well. In Figure 9c a replica prepared from a silica monolith with a monomodal mesopore size is represented, while in Figure 9d a replica from a bimodal silica monolith can be seen. The first is a conglomerate of crystalline particles with sizes in the range of 5−25 nm, with an average size of ∼15 nm. The second sample is a mixture of particles with bimodal size distribution, 3−7 nm (average ∼ 5 nm) and 15−35 nm (average ∼ 25 nm).

There are several direct and indirect methods to estimate the particle size. It can be approximated directly by taking an average from TEM images or indirectly from the BET surface area (if assuming unconnected spherical particles) and XRD peak broadening (by using the Scherrer equation). However, it has to clearly be stated that from XRD the size of crystallites is determined whereas from TEM and BET the size of particles is obtained, which sometimes consist of many crystallites and, therefore, represents more or less aggregates. The results are summarized in Table 2. It is clear from all methods that the SnO_2 replica has the smallest particle size, while the Mn_2O_3 has the largest when comparing replicas from the same starting silica monolith. However, when different silica monoliths are used as molds different

replica structures are obtained. Depending on if a monomodal or bimodal *mesopore* size distribution of the silica is used a monomodal or bimodal *particle* size distribution is obtained in the SnO_2 replicas. Furthermore, the respective particle sizes correlate very well with the mesopore size of the starting materials. Hence, it is clearly a negative replica of the mesostructure.

Furthermore, in Figure 9b one can clearly see the lattice fringes indicating atomic order in the SnO_2 particles. This can also be observed for the other oxides, which confirms that the replicas are fully crystalline (this could also be observed by XRD).

4. Conclusions

We have described a fairly general method for the preparation of macroporous/mesoporous monoliths of different metal oxides through nanocasting. On the macroscopic level the replicas are very similar to the parent SiO_2 monoliths, which can be seen on the macroscopic morphology of the monoliths and the macropore structure. One can say that they are positive replicas of the silica structure on this length scale. Therefore, it is easy to control the sizes of these simply by using different starting silica monoliths. However, on the nanometer scale the replica structures are negative replicas of the silica structure, implying that pores in the silica structure will become poor walls in the replica structure and vice versa. It was also demonstrated that the structure can be altered by using silica monoliths with different mesopore structures. However, depending on which metal oxide replica is prepared, small deviations in the structures can be observed on the nanometer scale. Co_3O_4 and SnO_2 will both pack closely to the SiO_2 surface and thus make a true replica of the silica mesopores. On the other hand, the manganese oxides do not interact with silica to a similar high degree and larger particles of the oxides will eventually block some of the mesopores or even deposit in the macropores. It is also clear that the final structures are dependent on the drying/decomposition temperature, the type of metal salt, the concentration, the air flow through the oven, and so forth, which must be optimized for each system. Finally, the metal oxide replicas are all fully crystalline and built up of nanocrystallites with a crystallite size which depends on the mesopore size of the silica monolith. This indicates that these novel metal oxide monoliths have a hierarchical structure and that it is possible to alter the sizes on several length scales independently.

Our present work is to expand the method to other metal oxides as well as to surface functionalize the monoliths. Reduction of the metal oxide monoliths to prepare porous metal monoliths is also a possibility to prepare other interesting properties.

Acknowledgment. The authors would like to warmly thank Mr. Bernd Spliethoff (MPI für Kohlenforschung) for conducting the TEM and Mr. Sami Areva and Mr. Mikael Järn (Dept. Phys. Chem., Åbo Akademi University) for the SEM/EDX measurements. The integrated EU project AIMs and the Academy of Finland (Grant HPM) are greatly acknowledged for financial support.

CM051880P